Ferrimagnetism in $Ni_4Nb_2O_9$

H. Ehrenberg, G. Wltschek, and H. Weitzel
Fachgebiet Strukturforschung, Fachbereich Materialwissenschaft, Technische Hoschschule Darmstadt, D-64287 Darmstadt, Federal Republic of Germany

F. Trouw
IPNS Division of the Argonne National Laboratory, 9700 South Cass Avenue, Argonne, Illinois 60439

J. H. Buettner, and T. Kroener
Forschungszentrum Karlsruhe, Institut fuer Technische Physik, P.O.B. 3640, D-76021 Karlsruhe, Federal Republic of Germany

H. Fuess
Fachgebiet Strukturforschung, Fachbereich Materialwissenschaft, Technische Hochschule Darmstadt, D-64287 Darmstadt, Federal Republic of Germany
(Received 10 May 1995)

For the *Pbcn* form of nickel diniobate $Ni_4Nb_2O_9$ ferrimagnetic ordering is observed below T_C = 76.1(1) K. Two models for the magnetic structure result in calculated intensities for the magnetic reflections, which are in satisfying agreement to the data observed in neutron powder diffraction. In both cases the magnetic structure consists of two ferromagnetic sublattices according to the two Ni sites, which are antiparallel to each other. One model belongs to the magnetic symmetry group $Pb'cn'$ with the moments aligned parallel [010] and the other one to $Pbc'n'$ with the moments parallel [100]. The absolute values of the magnetic moments, constrained to the same value for both sites, are determined to $|\mu| = 1.35(5)\mu_B$ (60 K) and $1.65(5)\mu_B$ (1.5 K) for both models. A compensation temperature of $T_{comp} = 33$ K is observed, and the magnetic properties can be explained by the competition between antiferromagnetic intrasite and intersite couplings using mean field approximation. In the paramagnetic region an averaged magnetic moment of $3.54(5)\mu_B$ is derived from the Curie-Weiss constant. These values are in good agreement with the predictions by Hund's rules for Ni^{2+}.

INTRODUCTION

For nickel diniobate $Ni_4Nb_2O_9$ two different modifications are reported. Both crystallize in orthorhombic symmetry groups, one in *Fd2d* (Ref. 1) with a larger unit cell ($Z = 32$) and the other one with a reduced unit cell ($Z = 4$) in *Pbcn*.[2] Its crystal structure can be described as a network of edge- and corner-sharing NiO_6 and NbO_6 octahedra dimers as shown in Fig. 1.[2] This paper is concerned with the magnetic structure and properties of the *Pbcn* form.

EXPERIMENT

The synthesis of nickel diniobate $Ni_4Nb_2O_9$ was carried out by subsolidus reaction of a mixture of Nb_2O_5 (99.99 % Aldrich) and NiO (99.99 % Aldrich) in ratio 1:4. The reactants were intimately mixed in an agate mortar under acetone, placed in a platinum crucible, and heated in flowing oxygen to 1450 °C at a rate of 240 °C/h. After 48 h the reaction product was cooled down at a rate of 120 °C/h to room temperature. Small trilling crystals of light green color and trifling impurities of NiO and $NiNb_2O_6$ were obtained.

The neutron diffraction experiments were performed at the spallation source of the IPNS Division at the Argonne National Laboratory. Intensity data were collected at the High Intensity Powder Diffractometer (HIPD) with two

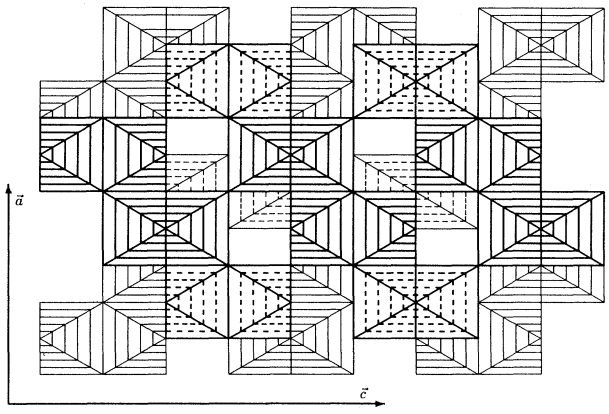

FIG. 1. Crystal structure of $Ni_4Nb_2O_9$ with view along [010]. The dashed octahedra contain Nb ions and the ones with drawn lines Ni ions.

detector banks at scattering angles of $2\Theta = 30°$ and 90°. Three diffraction patterns were recorded at 1.5 K, 60 K, and 150 K. For the purpose of data analysis the program GSAS by Larson and von Dreele was used.[3]

The specific heat was measured with a continuous adiabatic heating calorimeter, the magnetic susceptibility with an ac susceptometer ACS 7000 (Lakeshore), and the magnetizations using a superconducting quantum interference device (SQUID) (Quantum Design).

RESULTS

For the *Pbcn* form of $Ni_4Nb_2O_9$ one λ peak is observed in the specific heat at $T_C = 76.1(1)$ K; see Fig. 2. The magnetic ac susceptibility and its inverse are shown in Fig. 3. The huge susceptibility next to T_C and the Curie-Weiss temperature of $\Theta = -215(10)$ K indicate ferrimagnetic order, which turns out to be extremely weak. In the field dependence of the magnetization per ion a compensation temperature of $T_{comp} = 33$ K is confirmed by a linear behavior instead of hysteresis effects, which occur below and above T_{comp}; see Fig. 4.

In the neutron powder diffraction pattern recorded at 150 K [Fig. 5(a)] only nuclear reflections appear, and the crystal structure was refined by Rietveld analysis. The results are summarized in Table I using standard representation. No significant deviations from reported data[2] were detected. The Ni ions occupy two different crystallographic sites of octahedral coordination with bond lengths given in Table II. For both sites nine neighbours of Ni ions exist, which are bridged via one oxygen ion. They can be divided into three neighbors of the same site and six of the other. All possible superexchange paths are listed in Table III.

In the diffraction patterns recorded at 60 K and 1.5 K [Figs. 5(b), 5(c)] some intensities have increased compared to the 150 K data caused by contributions from magnetic scattering. No additional reflections occur, indicating that the magnetic unit cell is identical to the crystallographic one, i.e., $\vec{k} = 0$. In order to resolve the magnetic structure eight models have to be examined by symmetry considerations. The generators of the magnetic symmetry groups and the resulting types of magnetic order are given in Table IV. Only models 2, 3, and 7 are compatible with a ferromagnetic component of the magnetic structure, which is necessary to explain both the field dependence of magnetization as shown in Figs. 4(a), 4(c) and the huge susceptibility as shown in Fig. 3. The magnetic reflections of highest intensities are (002) and (004). Contributions to these reflections arise only from the projection of magnetic moments into the *ab* plane, resulting in an exclusion of model 3. For

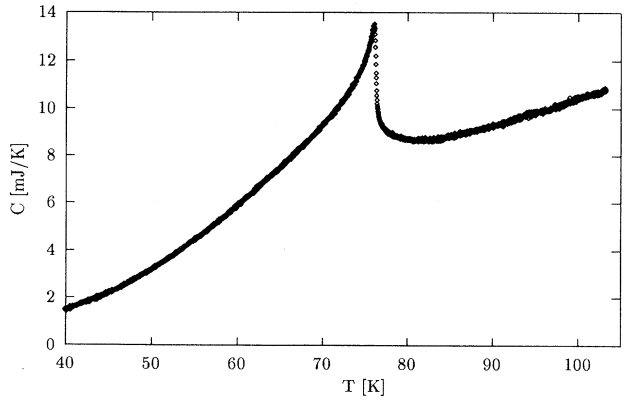

FIG. 2. Specific heat of $Ni_4Nb_2O_9$.

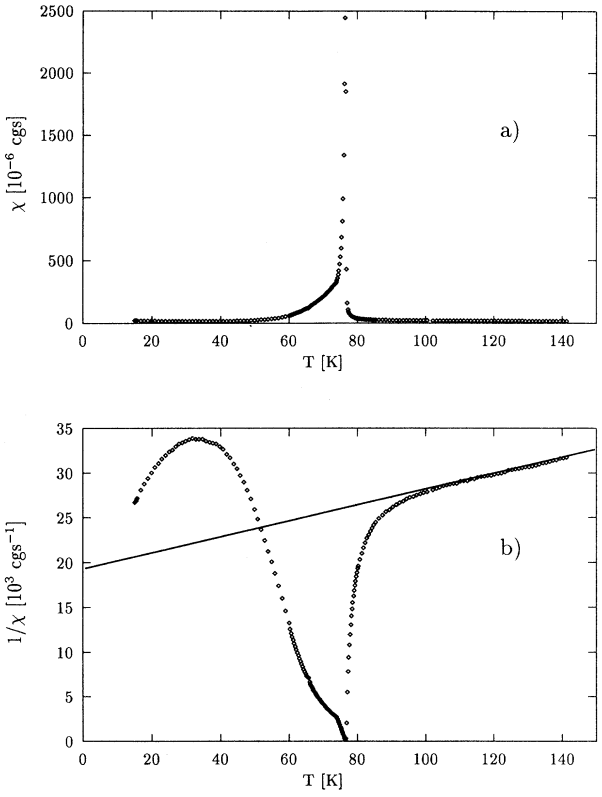

FIG. 3. (a) Magnetic ac susceptibility of $Ni_4Nb_2O_9$ and (b) the inverse ac susceptibility with a Curie-Weiss fit (drawn line) to the paramagnetic region. A dc field of 640 A/m was applied to $H_{ac} = 320$ A/m with $f = 333.3$ Hz.

TABLE I. Atomic parameters for $Ni_4Nb_2O_9$ at 150 K as derived from neutron powder diffraction.

Space group	*a* [Å]	*b* [Å]	*c* [Å]
Pbcn	8.7185(2)	5.0726(2)	14.2915(3)
Atom	*x*	*y*	*z*
Ni(1)	0.3391(3)	0.0008(9)	0.6878(1)
Ni(2)	0.3357(4)	0.9929(8)	0.5015(1)
Nb	0.0307(2)	0.0040(13)	0.8550(1)
O(1)	0	0.2854(13)	0.75
O(2)	0.1669(6)	0.1694(7)	0.9285(3)
O(3)	0.1630(6)	0.1748(8)	0.5975(3)
O(4)	0.1486(6)	0.1490(12)	0.2502(3)
O(5)	0.5008(5)	0.1671(10)	0.9155(4)

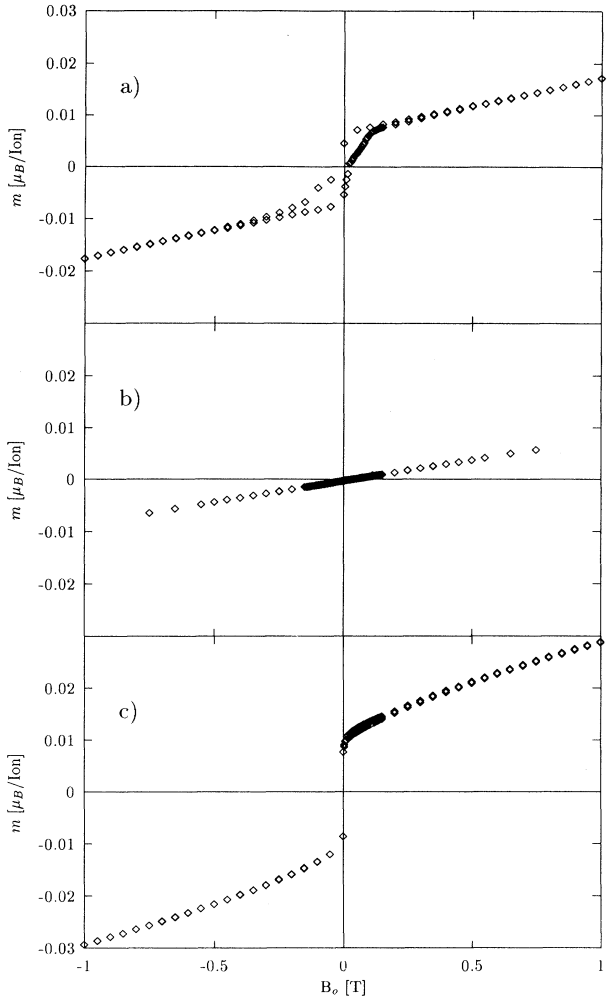

FIG. 4. Field dependence of the magnetization per ion at (a) 2 K, (b) 33 K, and (c) 76 K as derived from SQUID measurements.

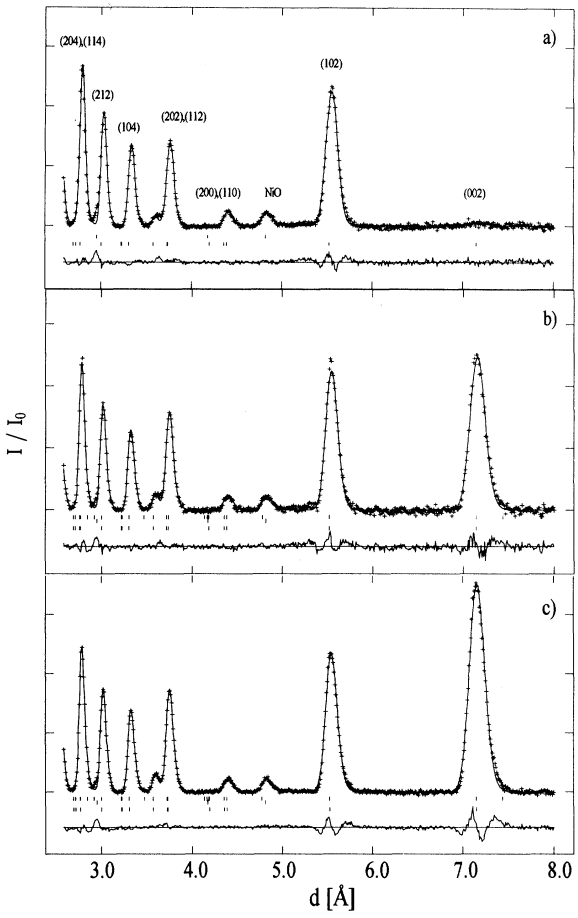

FIG. 5. Neutron diffraction patterns recorded at (a) 150 K, (b) 60 K and (c) 1.5 K. The bottom line of reflection markers belongs to the nuclear reflections of $Ni_4Nb_2O_9$ and the top line in (b) and (c) to the magnetic ones. The remaining markers belong to the NiO impurity.

both remaining models a spin configuration can be found with satisfying agreement of calculated total intensities and observed data at 1.5 K as summarized in Table V. The magnetic structure consists of two collinear ferromagnetic sublattices, which are antiparallel to each other for both models, but in $Pb'cn'$ the moments are aligned parallel [010] and in $Pbc'n'$ parallel [100]. The reflections with different intensities for both models are dominated by nuclear contributions, and very slight changes in the atomic parameters are sufficient to fade out these differences. That means that both models cannot be distinguished by unpolarized neutron powder diffraction. Magnetic susceptibility measurements on single crystals would provide the most information to resolve this uncertainty in the easy magnetization direction, but unfortu-

TABLE II. Bond lengths [Å] for the NiO_6 and NbO_6 octahedra in $Ni_4Nb_2O_9$ at 150 K.

Ni(1)-O(1)	1.988	Ni(2)-O(2)	1.983	Nb(1)-O(2)	1.794
Ni(1)-O(4)	1.991	Ni(2)-O(2)	2.006	Nb(1)-O(5)	1.935
Ni(1)-O(4)	2.033	Ni(2)-O(5)	2.054	Nb(1)-O(4)	1.975
Ni(1)-O(3)	2.098	Ni(2)-O(5)	2.060	Nb(1)-O(3)	2.016
Ni(1)-O(3)	2.191	Ni(2)-O(3)	2.118	Nb(1)-O(1)	2.088
Ni(1)-O(5)	2.200	Ni(2)-O(3)	2.236	Nb(1)-O(4)	2.304

TABLE III. Ni-Ni distances [Å] and angles [°] for all Ni-Ni pairs, which are coupled by super exchange via one oxygen for $Ni_4Nb_2O_9$ at 150 K.

Ni(1)-O(5)-Ni(2)	2.663	77.4
Ni(1)-O(3)-Ni(2)	2.663	73.9
Ni(1)-O(3)-Ni(2)	2.663	78.3
Ni(2)-O(5)-Ni(2)	2.866	88.3
Ni(2)-O(2)-Ni(2)	2.944	95.1
Ni(2)-O(3)-Ni(2)	2.944	85.0
Ni(1)-O(4)-Ni(1)	2.974	95.3
Ni(1)-O(3)-Ni(1)	2.974	87.8
Ni(1)-O(1)-Ni(1)	3.321	113.3
Ni(1)-O(5)-Ni(2)	3.919	133.9
Ni(1)-O(3)-Ni(2)	3.955	133.2
Ni(1)-O(3)-Ni(2)	4.006	135.1

TABLE IV. The eight different magnetic symmetry models with their generators and the resulting magnetic order. t means time reversal, AF antiferromagnetic, and $F\alpha$ denotes a ferromagnetic component α. 2_1 is $2(00\frac{1}{2})$ $\frac{1}{4}\frac{1}{4}z$.

No.	C_1	C_2	C_3	Magnetic symmetry group	Magnetic order
1	2_1	2	$\bar{1}$	$Pbcn$	AF
2	$2_1 \circ t$	2	$\bar{1}$	$Pb'cn'$	Fy
3	2_1	$2 \circ t$	$\bar{1}$	$Pb'c'n$	Fz
4	2_1	2	$\bar{1} \circ t$	$Pb'c'n'$	AF
5	2_1	$2 \circ t$	$\bar{1} \circ t$	$Pbcn'$	AF
6	$2_1 \circ t$	2	$\bar{1} \circ t$	$Pbc'n$	AF
7	$2_1 \circ t$	$2 \circ t$	$\bar{1}$	$Pbc'n'$	Fx
8	$2_1 \circ t$	$2 \circ t$	$\bar{1} \circ t$	$Pb'cn$	AF

nately all isolated crystals were at least triplets and much too small for this purpose. A difference in the absolute values of the two sublattice magnetizations is essential for the explanation of the magnetic properties, but too small to be resolved in the diffraction experiments. The constrained values are refined to $1.65(5)\mu_B$ (1.5 K) and $1.35(5)\mu_B$ (60 K) in both models. From a Curie-Weiss fit in the paramagnetic region the averaged magnetic moment of one Ni ion is calculated to $3.54(5)\mu_B$; see Fig. 3(b). This is a typical value for the $^3F_4$ ground state of Ni^{2+} as compared to the spin-only value $2.83\mu_B$ and the free-ion value of $5.59\mu_B$ derived from Hund's rules. The sublattice magnetization of $1.65\mu_B$ has to be compared to $g_0 m_S = 2\mu_B$, indicating that the spins are not completely ordered.

DISCUSSION

The explanation of the magnetic properties is based on the following Hamiltonian for an applied magnetic field $\vec{B}_0 = (0, 0, B_0)$:

$$\hat{H} = -\frac{1}{2}\sum_{i \neq j} J_{ij}\hat{\vec{S}}_i \cdot \hat{\vec{S}}_j + \frac{\mu_B}{\hbar}B_0 \sum_i g_i \hat{S}_i^z. \tag{1}$$

The first summation includes all pairs, which are coupled by superexchange via one oxygen as given in Table III. The Hamiltonian in a mean field approximation is readily derived to

$$\hat{H}_{\mathrm{mf}} = \frac{1}{2}\sum_{i \neq j} J_{ij}\langle S_i^z\rangle\langle S_j^z\rangle + \frac{\mu_B}{\hbar}\sum_i g_i \left(B_0 + B_e^{(i)}\right)\hat{S}_i^z, \tag{2}$$

with

$$B_e^{(i)} = -\frac{\hbar}{g_i \mu_B}\sum_j J_{ij}\langle S_j^z\rangle. \tag{3}$$

In the case of $Ni_4Nb_2O_9$ two ferromagnetic sublattices s_1 [Ni(1) site of Table I] and s_2 [Ni(2) site] exist, and both the Landé factors g_i and the magnetizations per ion m_i have to be distinguished only for the different sites:

$$\langle S_j^z\rangle = -\frac{\hbar}{g_i \mu_B} m_i, \quad j \in s_i, \quad i = 1, 2. \tag{4}$$

By splitting the summation in (3) into neighbors of the same and different site, the exchange field B_e can be written as

$$B_e^{(1)} = -\frac{\hbar^2}{g_1 \mu_B^2}\left(j_{11}\frac{m_1}{g_1} + j_{12}\frac{m_2}{g_2}\right), \tag{5}$$

$$B_e^{(2)} = -\frac{\hbar^2}{g_2 \mu_B^2}\left(j_{21}\frac{m_1}{g_1} + j_{22}\frac{m_2}{g_2}\right), \tag{6}$$

where the effective intra- and intersite couplings

$$j_{ij} = \sum_{k \in s_j} J_{ik}, \quad i, j = 1, 2, \tag{7}$$

have been introduced. For the ground state of Ni^{2+} ions the spin quantum number is $S = 1$, and the magnetizations per ion are determined by the Brillouin function B_1 in the following way:

$$m_i(T, B_0) = g_i \mu_B B_1\left(\frac{g_i \mu_B}{k_B T}\left[B_0 + B_e^{(i)}\right]\right). \tag{8}$$

In order to calculate the sublattice magnetizations for given values of temperature and external field, the Landé factors g_1, g_2 and the exchange constants j_{11}, j_{12}, j_{22}

TABLE V. The magnetic reflections of highest intensity for both models as compared to the nuclear contributions and the observed intensities.

(hkl)	d [Å]	I (nuclear)	I (model 2)	I (model 7)	I (observed)
(002)	7.144	3.1	180.0	182.8	185.5
(102)	5.525	108.5	20.7	12.7	129.7
(112)	3.735	70.4	21.1	39.4	Σ 197.0
(202)	3.720	72.4	35.9	10.2	
(004)	3.572	52.6	57.1	59.7	121.3
(104)	3.305	296.5	43.3	38.9	329.1
(212)	2.999	278.4	13.3	11.3	289.0

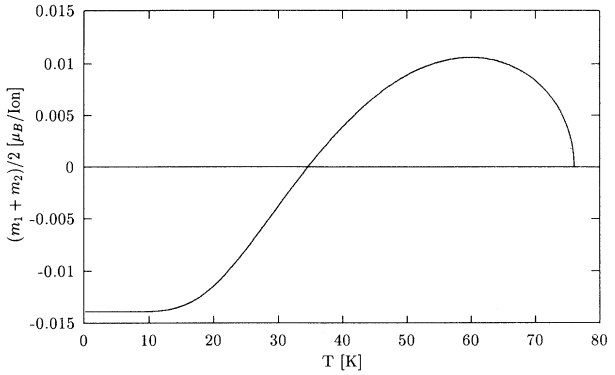

FIG. 6. Calculated magnetization per ion as function of temperature without an external field.

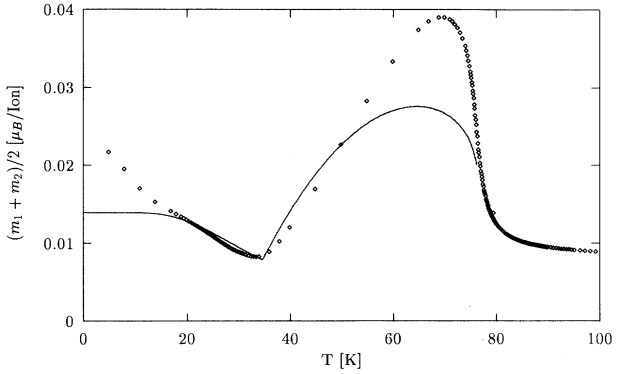

FIG. 7. Calculated and observed magnetization per ion as a function of temperature with an external field of $B_0 = 1$ T.

have to be known. They can be determined from experimental values as follows: Next to the transition temperature and in the limit of a weak external field ($B_0 \to 0$) the first term in the expansion of the Brillouin function is sufficient and spontaneous magnetization is possible below

$$T_C = \frac{\hbar^2}{3k_B}\left\{j_{11}+j_{22}+\left[(j_{11}-j_{22})^2+4j_{12}^2\right]^{\frac{1}{2}}\right\} = 76.1\,\mathrm{K}. \tag{9}$$

For high temperatures $T \gg T_C$ the susceptibility per ion obeys a Curie-Weiss law

$$\chi(T) = \frac{C}{T-\Theta}, \tag{10}$$

with Curie constant C and Weiss temperature Θ given by

$$C = (g_1^2+g_2^2)\frac{\mu_B^2}{3k_B} = 25.0\frac{\mu_B^2}{3k_B}, \tag{11}$$

$$\Theta = \frac{2}{3}\frac{\hbar^2}{k_B}\left(\frac{2j_{12}g_1g_2 - j_{22}g_1^2 - j_{11}g_2^2}{g_1^2+g_2^2} + j_{11} + j_{22}\right) = -215\,\mathrm{K}. \tag{12}$$

Besides these three equations the compensation temperature $T_{\mathrm{comp}} = 33$ K, defined by

$$m_1(T_{\mathrm{comp}}) + m_2(T_{\mathrm{comp}}) = 0 \quad \text{for} \quad B_0 = 0, \tag{13}$$

and the magnetization at this temperature for an applied field,

$$\frac{1}{2}\left[m_1(T_{\mathrm{comp}}) + m_2(T_{\mathrm{comp}})\right] = 8.45\times 10^{-3}\mu_B/\mathrm{ion} \quad \text{for} \quad B_0 = 1\ T, \tag{14}$$

are used for the determination of the model parameters to

$$g_1 = 3.52,\ g_2 = 3.55,\ j_{11} = -100\frac{k_BK}{\hbar^2},\ j_{12} = -218\frac{k_BK}{\hbar^2},\ j_{22} = -108\frac{k_BK}{\hbar^2}. \tag{15}$$

It turns out that all effective couplings are antiferromagnetic and dominated by the intersite coupling j_{12}, resulting in a ferrimagnetic structure. Even without an external field the small differences in the Landé factors and the intrasite couplings avoid the sublattice magnetizations compensating each other, except at the compensation temperature as shown in Fig. 6. It should be emphasized that compensation is only possible with the stronger intrasite coupling between the ions with the larger Landé factor. The difference in the sublattice magnetizations is always less than $0.015\mu_B$/ion and therefore one cannot decide which crystallographic site is the one with a larger Landé factor. In Fig. 7 the calculated and observed magnetizations per ion are compared for an applied field of $B_0 = 1$ T. Although the calculated maximum is too small and the increase at low temperatures not reproduced, a qualitative description of the magnetic properties of $Ni_4Nb_2O_9$ can be given by a mean field approach.

ACKNOWLEDGMENTS

This work has benefited from the use of the Intense Pulsed Neutron Source at Argonne National Laboratory. This facility is funded by the U.S. Department of Energy, BES-Materials Science, under Contract No. W-31-109-Eng-38. Support by the *Bundesminister für Bildung und Forschung* (Grant No. 03-FU3DAR) is also gratefully acknowledged.

---

[1] R. Wichmann and H. Mueller-Buschbaum, Z. Anorg. Allg. Chem. **525**, 135 (1985).

[2] R. Wichmann and H. Mueller-Buschbaum, Z. Anorg. Allg. Chem. **539**, 203 (1986).

[3] A. C. Larson and R. B. von Dreele, General Structure Analysis System, LANSCE, Los Alamos National Laboratory.